JACS
JOURNAL OF THE AMERICAN CHEMICAL SOCIETY
Communication
pubs.acs.org/JACS

Output Coupling of Perovskite Lasers from Embedded Nanoscale Plasmonic Waveguides

Yong Jun Li,[†] Yuanchao Lv,[†] Chang-Ling Zou,[‡] Wei Zhang,[†] Jiannian Yao,[†] and Yong Sheng Zhao*[,†]

[†]Key Laboratory of Photochemistry, Institute of Chemistry, Chinese Academy of Sciences, Beijing 100190, China

[‡]Key Laboratory of Quantum Information, Synergetic Innovation Center of Quantum Information & Quantum Physics, University of Science and Technology of China, Hefei, Anhui 230026, China

Supporting Information

ABSTRACT: Nanoscale lasers are ideal light-signal sources for integrated photonic devices. Most of the present lasers made of dielectric materials are restricted to being larger than half the wavelength of the optical field. Plasmon lasers made from metallic nanostructures can help to break the diffraction limit, yet they suffer from low optical pump efficiencies and low quality factors. Integrating dielectric lasers with plasmonic waveguides to construct hybrid material systems may circumvent these problems and combine the advantages of the two components. Here we demonstrate the nanoscale output of dielectric lasers via photon−plasmon coupling in rationally designed perovskite/silver heterostructures. The perovskite crystals offer the gain and high-Q cavity for low-threshold laser generation, while the embedded silver nanowires (AgNWs) help to output the lasing modes efficiently in the form of surface plasmons. The output coupling can be modulated by controlling the resonant modes of the two-dimensional perovskite microcavities. The results would pave an alternative avenue to ultrasmall light sources as well as fundamental studies of light−matter interactions.

Ultrasmall light sources, especially powerful and coherent electromagnetic energy, hold the key to emerging applications in on-chip integration of nanophotonics and nanoelectronics.[1] To date, wavelength-scale lasers have been achieved using various materials such as photonic crystals[2] and semiconductor nanowires.[3−5] However, their mode volumes and outputs are limited to being larger than $\sim(\lambda/2n)^3$ for three-dimensional (3D) cavities due to the diffraction limit.[6] Surface plasmon polaritons (SPPs), the propagating collective electron oscillations along the metal surface, can tightly confine light in metallic nanostructures,[7] which has inspired the design and fabrication of various nanolasers at subwavelength scale.[8−13] Nevertheless, the small mode volumes and high Ohmic losses of such lasers lead to small quality (Q) factors.[12] An alternative option is to integrate light sources with plasmonic waveguides by directing light emission into SPP modes. For instance, slot[14] and double-strip[15] plasmonic waveguides can be combined with a light-emitting diode platform to achieve subwavelength optical circuits. Therefore, by integrating a dielectric laser with a plasmonic waveguide, we might be able to simultaneously achieve the high-Q resonant cavity and the output of highly localized coherent light sources.[11]

Controlled growth of organic and inorganic crystals in the liquid phase has been proved to be a robust strategy to construct hybrid nanomaterials, such as axial[16] and branchlike heterostructures,[17] and may also be viable for the construction of the proposed dielectric−metal hybrid systems because this strategy is free of strict lattice matching and sophisticated epitaxial technology.[18] Organic−inorganic halide perovskites can grow into different structures, including films[19] and microscale cavities,[20] through diffusion and nucleation in the liquid or vapor phase. Therefore, by utilizing metallic nanostructures as the nucleation centers, we might achieve the integration of perovskite materials with plasmonic components. Furthermore, halide perovskites, with long carrier lifetimes and diffusion lengths,[21] are emerging as one of the most promising materials for photovoltaic technology.[22] These properties, along with high fluorescence yield and wavelength tunability, also make halide perovskites ideal materials for lasing.[23] Indeed, they have shown efficient optical gain and ultrastable amplified spontaneous emission at strikingly low thresholds.[19,20,23] Therefore, halide perovskites might be ideal candidates for construction of hybrid systems for high-performance microscale lasers and their subwavelength output.

Here we propose a strategy for the highly localized output of perovskite lasers from metallic SPP waveguides embedded in the perovskite microcrystal cavities. The site-specific growth of $CH_3NH_3PbBr_3$ perovskite was induced on the surfaces of preloaded silver nanowires (AgNWs), which act as the preferential nucleation centers, to form a unique type of hybrid structure with part of each AgNW well embedded in a perovskite microcrystal. The perovskite microcrystals serve as both the gain medium and the optical resonant cavity for the low-threshold lasing upon irradiation with a pump light, and the lasing modes can be output at subwavelength scale by efficiently launching the propagating SPP modes in the embedded AgNWs. By selectively utilizing the whispering gallery or Fabry−Pérot resonant modes of the perovskite microcavities, we can modulate the lasing feature from the perovskite crystals and hence the output coupling from the AgNWs as well. The solidly connected embedded structures not only ensure a stable laser output that is insensitive to mechanical vibrations but also provide a

Received: December 7, 2015
Published: February 5, 2016

DOI: 10.1021/jacs.5b12755
J. Am. Chem. Soc. 2016, 138, 2122−2125

convenient approach for manipulating the plasmonic nanowires by way of monolithic translation.

The achievement of laser output by SPPs is schematically illustrated in Figure 1A. A nanoscale metal wire is partially embedded in a dielectric microcavity, where the lasing emission is generated with an optical pump. The embedded section can solidly bind them together to enable the efficient launching of SPPs on the metal wire surface by the amplified light in the dielectric phase, and the created SPPs propagate along the metal nanowire and are output from the distal ends as an ultrasmall coherent light source. In this work, chemically synthesized AgNWs were utilized to support the SPPs because of their atomically smooth surfaces (Figure S1) and reduced propagation losses.[24] AgNWs with a diameter of about 180 nm were utilized as plasmonic waveguides to support the SPP modes. The inorganic−organic halide perovskite compound was used to achieve low-threshold dielectric lasers because of its large absorption coefficient, ultralow bulk defect density, and slow Auger recombination.[19] $CH_3NH_3PbBr_3$ (Figure 1B) was selected because its fluorescent wavelength region (500−600 nm; Figure S2) makes it effective to launch the SPPs in AgNWs. In addition, this compound exhibits very good chemical stability under oxygen compared with other halide perovskites, such as $CH_3NH_3PbI_3$.[25]

The heterostructures were prepared by embedding AgNWs in $CH_3NH_3PbBr_3$ during crystal growth in the liquid phase (Figure S3). In a typical preparation, AgNWs dispersed in ethanol (2 mg mL^{-1}) were first drop-cast onto a quartz wafer, and then 0.5 mL of $CH_3NH_3PbBr_3$ solution (γ-butyrolactone, 0.03 mmol L^{-1}) was dispersed on the substrate preloaded with AgNWs. With the gradual evaporation of the solvent, the perovskite nucleated on the surfaces of the AgNWs and subsequently grew into microcrystals, and as a result, perovskite/Ag heterostructures were obtained and dispersed on the substrates for the subsequent characterizations. Typical scanning electron microscopy (SEM) images (Figure 1C,D) clearly show that the AgNWs are partially embedded in the perovskite microstructures, which makes it possible to launch SPPs in the AgNWs. The crystalline $CH_3NH_3PbBr_3$ structures (Figure S4) with lengths and widths of several micrometers and a height of about 700 nm (see the atomic force microscopy (AFM) image in the Figure 1D inset) may serve as high-Q cavities for low-threshold laser generation. The green emission from the perovskite crystals (Figure 1E) is beneficial for efficiently launching the SPPs with low propagation loss. The bodies of AgNWs are nonluminous, while small bright green spots (marked with white circles) were observed at the AgNW distal ends. These results not only exhibit the efficient photon−plasmon coupling at the embedded sections but also indicate the typical feature of the SPP waveguide, which can be utilized for the propagation of optical signals.[17]

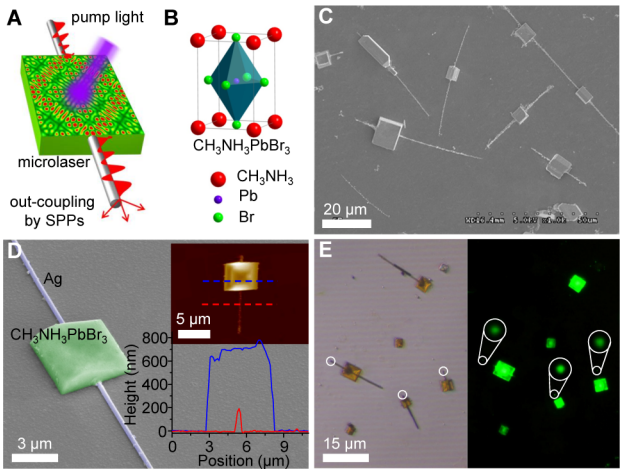

Figure 1. (A) Schematic illustration of an embedded dielectric/metal heterostructure for plasmonic output of dielectric laser. (B) Crystal structure of the selected dielectric material, $CH_3NH_3PbBr_3$. (C, D) SEM images of the perovskite/Ag heterostructures. Insets: AFM image and corresponding cross-section profiles of a typical heterostructure. (E) Bright-field (left) and PL (right) microscopy images of the heterostructures excited with the UV band of a mercury lamp (330−380 nm). Green points magnified in white circles are the result of scattering of SPPs at the AgNW distal ends.

To controllably fabricate the heterostructures for subwavelength laser output, we investigated the growth process by monitoring their temporal morphology during the liquid-phase assembly. In the initial stage, 30 min after drop-casting of the solution, perovskite crystals with sizes of tens of nanometers started to appear on the surfaces of the AgNWs (Figure 2A).

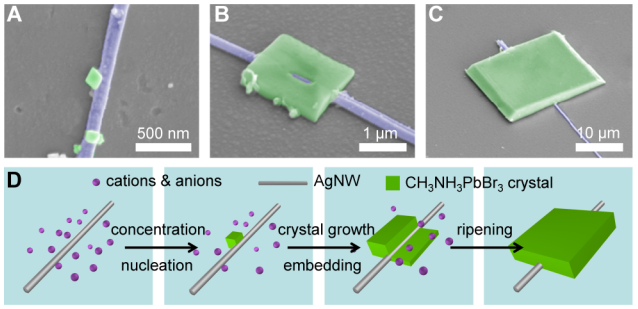

Figure 2. (A−C) False-color SEM images of the observed intermediates obtained at different growth stages: (A) 0.5 h; (B) 4 h; (C) 8 h. (D) Illustration of the growth process of the embedded perovskite/Ag heterostructures.

With the growth of $CH_3NH_3PbBr_3$, the AgNWs were gradually embedded in the crystals (Figure 2B). Finally, typical heterostructures (Figure 2C) were obtained when the growth reached a thermodynamic equilibrium after ripening for about 8 h. On the basis of these observations, we have illustrated the growth process in Figure 2D.

The AgNWs with small curvature radii and higher surface energies play the role of condensation centers to facilitate the nucleation of $CH_3NH_3PbBr_3$,[26] and isolated perovskite nanocrystals formed on the AgNW surfaces in the earlier stage. Subsequently, epitaxial growth of the preformed crystals occurred in the liquid phase, which could gradually embed the AgNWs. The embedding of AgNWs can avoid major disruption of the lattice structure and reduce the overall interfacial energy,[18,27] which is crucial for the stability of the heterostructures. As a result, structures with sharp junctions and smooth surfaces were obtained after exhaustion of the ions in the evaporating droplets. In the event of multiple nucleation sites on a AgNW, the larger crystal would inhibit the growth of the smaller neighboring ones and even "engulf" them as additional material sources to reduce the surface energy.[18] Therefore, each AgNW was eventually embedded in a single microscale perovskite crystal. Following this growth process, we can control the size of the perovskite crystal part in the heterostructure to get perovskite microcavities with tunable resonant lengths. For example, the length of the perovskite crystal edge can be

DOI: 10.1021/jacs.5b12755
J. Am. Chem. Soc. 2016, 138, 2122−2125

increased from ~2 to 20 μm by changing the concentration of the solution from 0.01 to 0.06 mmol L^{-1} (see Figure S5).

These heterostructures with good connection between the perovskite crystal and AgNW offer an ideal platform for investigating the output coupling of lasers via propagated SPPs. As displayed in Figure 3A, when a 400 nm femtosecond-pulsed

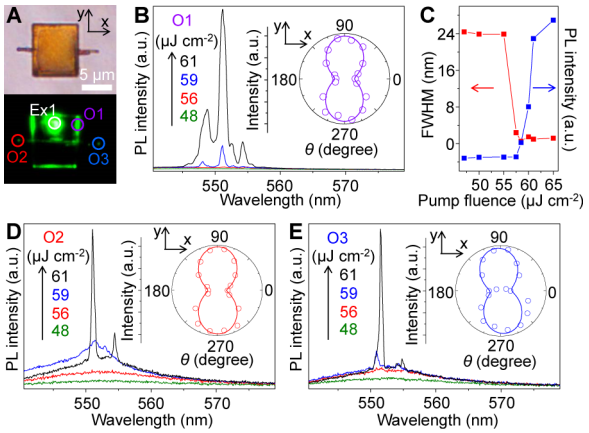

Figure 3. (A) Bright-field and PL images of a perovskite/Ag heterostructure locally excited at the perovskite crystal (Ex1, marked with a white circle). O1, O2, and O3 denote the spectra collection positions at the perovskite crystal edge and AgNW tips, respectively. (B, D, E) PL spectra collected from (B) the perovskite crystal and (D, E) the AgNW tips as functions of the pump fluence. Insets: polarization profiles of the emission intensities of the lasing modes. (C) Plots of the PL peak intensity (blue line) and fwhm (red line) vs the pump fluence.

laser beam (150 fs, 1 kHz) was focused on the perovskite crystal (see Figure S6 for the setup), bright photoluminescence (PL) emissions were observed from the crystal edges. A series of sharp peaks were found in the collected PL spectra taken from the edge of the perovskite crystal (O1), as shown in Figure 3B. With increasing pump fluence (per pulse), the PL intensity of the 551 nm peak in the gain region was dramatically amplified. Both the pump fluence dependence of the PL intensities and the full width at half-maximum (fwhm) (Figure 3C) show a nonlinear threshold behavior around 59 μJ cm^{-2}, and a typical three-stage transition comprising spontaneous emission, amplified spontaneous emission, and full lasing oscillation was observed, which confirmed the lasing action of the $CH_3NH_3PbBr_3$ crystal. These laser modes output from O1 were polarized perpendicular to the AgNW (Figure 3B inset).

In the heterostructures, the 2D perovskite cavities may offer in-plane optical modes for SPP launching. This launching scheme is more promising for on-chip coupling and guiding of optical signals than those involving prisms or microscope objectives. More importantly, the momentum of the coherent photons, as either Fabry–Pérot (F–P) mode or whispering-gallery mode (WGM) emitted from the perovskite cavity, would have a very high probability to match that of the propagating SPPs in the AgNW. As shown in Figure 3A, SPPs were efficiently launched and re-emitted as photons from the two AgNW distal ends (O2 and O3). The spectra collected from the AgNW tips (Figure 3D,E) show the same peaks at 551 and 554 nm as in the spectrum obtained at the $CH_3NH_3PbBr_3$ crystal edge. It should be noted that the peak with a wavelength of about 548.5 nm was almost "filtered out" by the AgNW as a result of the larger Ohmic losses of the SPP mode with higher energy,[28] which provides an alternative approach to single-mode nanolasers. The polarization measurements (Figure 3D,E insets) reveal that the light output from the wire tips maintained the polarizing characteristic of the cavity modes, i.e., all of the modes were polarized perpendicular to the AgNW. Therefore, the heterostructures reported here can well be utilized to achieve efficient outcoupling of the perovskite lasers via SPPs without obviously changing the intrinsic properties (wavelength, polarization, etc.).

The efficient and undistorted coupling between the cavity modes and the SPPs indicates that it is possible to modulate the output from the AgNWs by changing the lasing feature of the perovskite microcavity. As shown in Figure 4A, when the pump

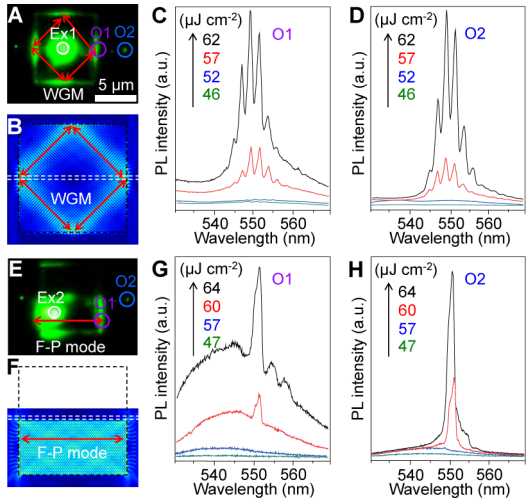

Figure 4. (A, E) PL images of the perovskite/Ag heterostructure locally excited at different positions of the perovskite crystal (Ex1 and Ex2, marked with white circles). O1 and O2 denote the positions for the spectra collection at the perovskite crystal edge and AgNW tip, respectively. (B, F) Numerically simulated electric field intensity ($|E|^2$) distributions in the whole perovskite crystal (B) and in the bottom half of the heterostructure (F). The white dashed lines indicate the orientation of the AgNW. (C, D) Spectra collected from the WGM cavity edge and the AgNW tip, respectively. (G, H) Spectra collected from the F–P cavity edge and the AgNW tip, respectively.

laser was focused at the middle area of the perovskite crystal, bright outcoupled emissions were observed from all four edges, indicating the formation of a typical WGM resonant cavity.[20] The simulated electric field intensity distribution (Figure 4B) reveals that the optical fields are well-confined inside the cavity and reflected between the adjacent polygonal facets to effectively support the WGMs. The preferential formation of the WGMs is attributed to the higher Q factor (~855) compared with that of the F–P modes (~440). Figure 4C shows the PL spectra collected from the crystal edge marked as O1 in Figure 4A with increasing pump fluence. The relationship between the mode spacing ($\Delta\lambda$) and the wavelength (λ) satisfies the equation of WGM theory, $\Delta\lambda = \lambda^2/nL_{IR}$, where n is the group refractive index (Figure S7) and L_{IR} is the length of the internal reflection path. The calculated L_{IR} (22.5 μm) is in good accordance with the length of the actual path (22.6 μm), marked with the red double-headed arrows in the PL image (Figure 4A). Figure 4D illustrates the corresponding spectra synchronously collected from the distal end of the AgNW (O2), which reveals that multiple laser modes were obtained from the silver wire without remarkably changing the features of the WGMs in the perovskite cavity.

When the laser beam was focused not at the middle but instead at one side of the silver wire (the bottom part), the square

DOI: 10.1021/jacs.5b12755
J. Am. Chem. Soc. 2016, 138, 2122–2125

perovskite crystal was divided into two rectangular resonant cavities by the embedded AgNW, and the outcoupled emissions could be observed only from the left and right edges of the excited bottom cavity (Figure 4E). This suggests that the F−P modes formed in the bottom dominated the resonance (Figure 4F) because of the strong scattering of the AgNW. Figure 4G shows that the PL spectra collected from the crystal edge (O1) exhibit rather different mode features from those shown in Figure 4C: $\Delta\lambda$ was increased to ~3.2 nm, which is much larger than that of the WGMs (~2.3 nm). Since the length of the measured perovskite crystal edge is $L \approx 8$ μm, $\Delta\lambda$ and λ satisfy the equation $\lambda^2/\Delta\lambda = 2nL$ (for more details, see Figure S7), further testifying to the formation of the F−P mode microcavity with this pump style.[29] The modulated output coupling of the modes via SPPs was obviously observed at the AgNW ends (the green spots in Figure 4E), and more interestingly, the spectra collected from O2, shown in Figure 4H, demonstrate that a nearly single-mode laser was outcoupled from the tip of the AgNW as a result of the differentiation in the Ohmic losses of the SPPs.

The outcoupling efficiencies (η) between the photonic mode and the plasmonic mode were calculated using numerical simulation (see the Supporting Information): for the F−P modes, $\eta \approx 1.65\%$, while for the WGMs, $\eta \approx 1.46\%$. The higher η of F−P modes can be understood in terms of wave vector matching.[7] The momentum along the direction of the AgNW for the F−P modes is larger than that for the WGMs, and thus, the F−P modes can better match the plasmonic waveguide mode, resulting in a higher coupling efficiency. The coupling efficiency can be further improved by embedding the AgNW in the middle of the perovskite microplate to get better field overlap or changing the wire direction to get better wave vector matching.

In summary, we have rationally designed and constructed a type of embedded perovskite/Ag heterostructure for the realization of nanoscale laser output. The heterostructures were successfully synthesized by using AgNWs as centers for site-specific nucleation and crystal growth of perovskite. In the heterostructures, the perovskite crystals can serve as both the gain medium and the optical resonant cavity for low-threshold lasing. The lasing modes can be output via SPPs by well-retaining the intrinsic lasing characteristics, which enabled us to modulate the output by controlling the resonant modes of the perovskite microcavities. We believe that these results will provide a good inspiration for the design of hybrid material systems for ultrasmall coherent light sources, which is indispensible for decreasing device dimensions in optical information processing.

■ ASSOCIATED CONTENT

Supporting Information

The Supporting Information is available free of charge on the ACS Publications website at DOI: 10.1021/jacs.5b12755.

Experimental details and additional data (PDF)

■ AUTHOR INFORMATION

Corresponding Author

*yszhao@iccas.ac.cn

Notes

The authors declare no competing financial interest.

■ ACKNOWLEDGMENTS

This work was supported by the National Natural Science Foundation of China (21125315, 21533013, 21521062), the Ministry of Science and Technology of China (2012YQ120060), and the Strategic Priority Research Program of the Chinese Academy of Sciences (XDB12020300).

■ REFERENCES

(1) Noda, S. *Science* **2006**, *314*, 260.
(2) Park, H.-G.; Kim, S.-H.; Kwon, S.-H.; Ju, Y.-G.; Yang, J.-K.; Baek, J.-H.; Kim, S.-B.; Lee, Y.-H. *Science* **2004**, *305*, 1444.
(3) Huang, M. H.; Mao, S.; Feick, H.; Yan, H.; Wu, Y.; Kind, H.; Weber, E.; Russo, R.; Yang, P. *Science* **2001**, *292*, 1897.
(4) Duan, X.; Huang, Y.; Agarwal, R.; Lieber, C. M. *Nature* **2003**, *421*, 241.
(5) Yan, H.; He, R.; Johnson, J.; Law, M.; Saykally, R. J.; Yang, P. *J. Am. Chem. Soc.* **2003**, *125*, 4728.
(6) Zheludev, N. I.; Prosvirnin, S.; Papasimakis, N.; Fedotov, V. *Nat. Photonics* **2008**, *2*, 351.
(7) Yan, R.; Pausauskie, P.; Huang, J.; Yang, P. *Proc. Natl. Acad. Sci. U. S. A.* **2009**, *106*, 21045.
(8) Bergman, D. J.; Stockman, M. I. *Phys. Rev. Lett.* **2003**, *90*, 027402.
(9) Noginov, M. A.; Zhu, G.; Belgrave, A. M.; Bakker, R.; Shalaev, V. M.; Narimanov, E. E.; Stout, S.; Herz, E.; Suteewong, T.; Wiesner, U. *Nature* **2009**, *460*, 1110.
(10) Oulton, R. F.; Sorger, V. J.; Zentgraf, T.; Ma, R.-M.; Gladden, C.; Dai, L.; Bartal, G.; Zhang, X. *Nature* **2009**, *461*, 629.
(11) Wu, X.; Xiao, Y.; Meng, C.; Zhang, X.; Yu, S.; Wang, Y.; Yang, C.; Guo, X.; Ning, C.; Tong, L. *Nano Lett.* **2013**, *13*, 5654.
(12) Lu, Y.-J.; Kim, J.; Chen, H.-Y.; Wu, C.; Dabidian, N.; Sanders, C. E.; Wang, C.-Y.; Lu, M.-Y.; Li, B.-H.; Qiu, X.; Chang, W.-H.; Chen, L.-J.; Shvets, G.; Shih, C.-K.; Gwo, S. *Science* **2012**, *337*, 450.
(13) Berini, P.; De Leon, I. D. *Nat. Photonics* **2012**, *6*, 16.
(14) Huang, K. C. Y.; Seo, M.-K.; Sarmiento, T.; Huo, Y.; Harris, J. S.; Brongersma, M. L. *Nat. Photonics* **2014**, *8*, 244.
(15) No, Y.-S.; Choi, J.-H.; Ee, H.-S.; Hwang, M.-S.; Jeong, K.-Y.; Lee, E.-K.; Seo, M.-K.; Kwon, S.-H.; Park, H.-G. *Nano Lett.* **2013**, *13*, 772.
(16) Yan, Y.; Zhao, Y. S. *Chem. Soc. Rev.* **2014**, *43*, 4325.
(17) Li, Y. J.; Yan, Y.; Zhang, C.; Zhao, Y. S.; Yao, J. *Adv. Mater.* **2013**, *25*, 2784.
(18) Sindoro, M.; Feng, Y. H.; Xing, S. X.; Li, H.; Xu, J.; Hu, H. L.; Liu, C. C.; Wang, Y. W.; Zhang, H.; Shen, Z. X.; Chen, H. Y. *Angew. Chem., Int. Ed.* **2011**, *50*, 9898.
(19) Xing, G. C.; Mathews, N.; Lim, S. S.; Yantara, N.; Liu, X. F.; Sabba, D.; Gratzel, M.; Mhaisalkar, S.; Sum, T. C. *Nat. Mater.* **2014**, *13*, 476.
(20) Zhang, Q.; Ha, S. T.; Liu, X. F.; Sum, T. C.; Xiong, Q. H. *Nano Lett.* **2014**, *14*, 5995.
(21) Xing, G. C.; Mathews, N.; Sun, S. Y.; Lim, S. S.; Lam, Y. M.; Gratzel, M.; Mhaisalkar, S.; Sum, T. C. *Science* **2013**, *342*, 344.
(22) Zhou, H.; Chen, Q.; Li, G.; Luo, S.; Song, T.-B.; Duan, H.-S.; Hong, Z.; You, J.; Liu, Y.; Yang, Y. *Science* **2014**, *345*, 542.
(23) Zhu, H.; Fu, Y.; Meng, F.; Wu, X.; Gong, Z.; Ding, Q.; Gustafsson, M. V.; Trinh, M. T.; Jin, S.; Zhu, X. Y. *Nat. Mater.* **2015**, *14*, 636.
(24) Ditlbacher, H.; Hohenau, A.; Wagner, D.; Kreibig, U.; Rogers, M.; Hofer, F.; Aussenegg, F. R.; Krenn, J. R. *Phys. Rev. Lett.* **2005**, *95*, 257403.
(25) Zhang, S.; Audebert, P.; Wei, Y.; Al Choueiry, A.; Lanty, G.; Bréhier, A.; Galmiche, L.; Clavier, G.; Boissiere, C.; Lauret, J.-S.; Deleporte, E. *Materials* **2010**, *3*, 3385.
(26) Zhao, Y. S.; Zhan, P.; Kim, J.; Sun, C.; Huang, J. *ACS Nano* **2010**, *4*, 1630.
(27) Peng, Z.; Yang, H. *Nano Today* **2009**, *4*, 143.
(28) Shegai, T.; Huang, Y.; Xu, H.; Käll, M. *Appl. Phys. Lett.* **2010**, *96*, 103114.
(29) Liu, X.; Zhang, Q.; Xiong, Q. H.; Sum, T. C. *Nano Lett.* **2013**, *13*, 1080.

DOI: 10.1021/jacs.5b12755
J. Am. Chem. Soc. 2016, 138, 2122−2125